Treatment Planning and Image Guidance for Radiofrequency Ablation of Large Tumors

Hongliang Ren, *Member, IEEE*, Enrique Campos-Nanez, Ziv Yaniv, *Member, IEEE*, Filip Banovac, Hernan Abeledo, Nobuhiko Hata, and Kevin Cleary, *Member, IEEE*

***Abstract*—This article addresses the two key challenges in computer-assisted percutaneous tumor ablation: planning multiple overlapping ablations for large tumors while avoiding critical structures, and executing the prescribed plan. Toward semiautomatic treatment planning for image-guided surgical interventions, we develop a systematic approach to the needle-based ablation placement task, ranging from preoperative planning algorithms to an intraoperative execution platform. The planning system incorporates clinical constraints on ablations and trajectories using a multiple objective optimization formulation, which consists of optimal path selection and ablation coverage optimization based on integer programming. The system implementation is presented and validated in both phantom and animal studies. The presented system can potentially be further extended for other ablation techniques such as cryotherapy.**

***Index Terms*—Image guidance, open source, optimization, radiofrequency ablation (RFA), treatment planning.**

I. Introduction

THE latest statistics from the World Health Organization indicates that lung and liver cancer are among the top five most frequent cancer related deaths worldwide [1]. Percutaneous radiofrequency ablation (RFA) has emerged as a commonly used technique for the minimally invasive treatment of numerous organ cancers [2], including lung and liver. Though surgical resection provides the best way to treat cancer, it is estimated that only 10–15% of patients with lung or liver neoplasms are surgical candidates [3], [4], due to the extent of the disease or concurrent medical conditions. Approximately 80% of unresectable tumors may be amenable to image-guided ablative techniques, which have been established as primary ablative procedures at most institutions.

The current tumor ablation techniques use needle-like probes that deliver "thermotherapy" to kill the cancerous tissue. These probes either increase tissue temperature by techniques such as focused ultrasound, laser, radiofrequency, and microwave, or decrease tissue temperature by cryotherapy [5].

Two important clinical considerations are tumor size and accessibility to the lesion. Multiple overlapping ablations need to be planned to cover irregular and large tumors through a series of single probe ablations. In addition, the planned ablations should be accessible by the needle-based probe, should avoid critical structures, and minimize damage to healthy tissue.

Manual treatment planning and execution is dependent on the operator's experience and relies on a trial and error approach, which is error prone and time consuming without the assistance of semiautomatic planning and navigation. To address the aforementioned key challenges, this article focuses on a semiautomatic approach for RFA of liver tumors. The primary contribution in this article is the systematic approach that incorporates practical clinical constraints in planning and navigation.

The rest of this paper is organized as follows. Section II summarizes the challenges, significance and related work in RFA procedures. Section III presents the proposed system approach, which is validated in Section IV. Finally, Section V concludes the paper.

II. Significance and Related Work

A. Clinical Concerns and Challenges

The current procedure of RFA mainly has two clinical concerns described as follows.

1) Adequate Ablation Coverage of the Tumor: Despite the availability of larger electrodes, many procedures require multiple ablations to obtain the desired ablation margin. Multiple ablations are difficult to execute as there is no good way to visualize the overlapping areas or to distinguish ablated areas from nonablated ones. Due to the lack of real-time image guidance, repeated insertions and positioning of the electrode may be required to hit the target lesion. Unablated tissue containing residual tumor may result in tumor recurrence. Residual tumor tissue often grows in scattered, nodular, or eccentric patterns [6],

Manuscript received October 19, 2012; revised May 17, 2013; accepted October 14, 2013. Date of publication October 24, 2013; date of current version May 1, 2014. This work was supported in part by the U.S.A. National Institutes of Health (NIH) under Grant 7R01CA124377-05 and in part by Singapore Academic Research Fund, under Grant R397000139133.

H. Ren is with the Department of Biomedical Engineering, National University of Singapore, 119077 Singapore, and was with the Bioengineering Initiative, Sheikh Zayed Institute for Pediatric Surgical Innovation, Children's National Medical Center, Washington, DC 20310, USA (e-mail: ren@nus.edu.sg).

E. Campos-Nanez is with the Epsilon Group, An Alere Inc. Company, 615 Woodbrook Dr., Suite B, Charlottesville, VA 22901, USA (e-mail: ecamposn@gmail.com).

Z. Yaniv and K. Cleary are with the Bioengineering Initiative, Sheikh Zayed Institute for Pediatric Surgical Innovation, Children's National Medical Center, Washington, DC 20310 USA (e-mail: kcleary@cnmc.org, zyaniv@cnmc.org).

F. Banovac is the Chief of Interventional Radiology, Department of Radiology, Georgetown University Hospital, Washington, DC 20007, USA (e-mail: fb2@gunet.georgetown.edu).

H. Abeledo is with the Department of Engineering Management and Systems Engineering, The George Washington University, Washington, DC 20052, USA (e-mail:abeledo@gwu.edu)

N. Hata is with the Surgical Planning Laboratory, Department of Radiology, Brigham and Women's Hospital and Harvard Medical School, Boston, MA 02115 USA (e-mail: hata@bwh.harvard.edu).

Color versions of one or more of the figures in this paper are available online at http://ieeexplore.ieee.org.

Digital Object Identifier 10.1109/JBHI.2013.2287202

making it difficult to treat after an initial ablation. Some studies have shown that complete necrosis of the tumor was achieved in only 29%–47.6% of lesions with diameters of 3.1 cm or greater [7].

2) Accurate Real-Time Targeting: RFA typically relies on image guidance to manually place the radiofrequency needle within the tumor, such as ultrasound for guiding liver tumor ablation [8], and computed tomography (CT) for guiding lung tumor ablation. However, ultrasound imaging can be problematic for monitoring the ablation region due to hyperechogenicity [7] and imaging artifacts [9], especially in the presence of a metallic RFA probe. In comparison, CT offers better imaging quality but increases the radiation exposure to the patient and potentially the operator. To avoid radiation, one solution is to employ a tracking system to obtain the relative position between ablation probe and target, by landmark registration to a preoperative CT image [10]. This approach assumes the target organ deformation is acceptable for treatment purposes by using preoperative images for intraoperative treatment.

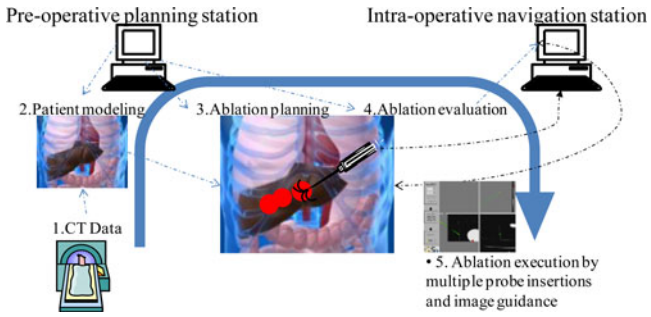

Fig. 1. Overall system schematic of a planning and image-based navigation system for tumor ablation: first in (block 1), the CT data are acquired for diagnosis and for patient specific modeling (block 2), which is done using a semiautomatic segmentation approach. Given identified entry points, critical structures, and tumor regions, the ablation planning (block 3) is performed by the preoperative planning station and the planned ablation spheres are overlaid in the scene with evaluation (block 4) on the coverage of the whole tumor while avoiding critical zone. Then, the surgical navigation (block 5) is performed using an image-guided surgery navigation platform (IGSTK, www.igstk.org) with fiducial marker registration to the preoperative CT scans. (Refer to the web version of this paper for the color figure.)

B. Prior Art on Computerized Treatment Planning for Overlapping Ablations

Planning of ablation procedures has been previously addressed by several groups. Baegert [11] employed a visibility graph method to optimize the entry point and avoid the critical structures, but did not address overlapping ablation issues. Overlapping spherical ablations have been studied by Dodd and Chen [12], [13]. Dodd [13] developed geometrical models to cover spherical tumors including a margin. Chen [12] explores an alternative approach by inscribing a regular polyhedron in the target sphere and circumscribing each face of the polyhedron with an ablation sphere. Yang *et al*. [14] focused on the robotic ablation system development and suggested a voxel growing algorithm for the large tumor treatment. Villard *et al.* [11] used a local search optimization technique to place a single ablation. Butz *et al*. [15] addressed several key issues in cryotherapy: finding a feasible trajectory, ablating all cancerous cells, and minimizing the damage to healthy tissue. A treatment measure was proposed to guide the plan optimization procedures. However, the optimization of multiple overlapping ablations was not addressed.

We further extended the problem in this article to develop a clinically robust treatment planning system by incorporating realistic constraints that are encountered in clinical practice but were not fully addressed before, including: 1) relaxation of the assumption of spherical tumors, i.e., no preselected geometric models of particular arrangements on tumors and 2) minimize the number of probe insertions and ablations while covering all tumor regions. Most tumors are not spherical and it is often not practical to regularly space overlapping ablations due to other nearby anatomical structures that should be avoided. Also, the number of probe insertions that can be performed in practice is limited by time considerations and the risk of complications with each insertion.

Earlier investigations were also done by our group [10], [16] and two approaches were proposed for treatment planning. Powell's method and simulated annealing algorithms [16] were used to find the solution for synthetic tumor data based on precomputed mask volumes and Euclidean distance transform. In that work, we were only concerned with tumor coverage and did not limit the number of probe insertions nor attempt to minimize damage to healthy tissue. Furthermore, the open-source image-guided surgery toolkit (IGSTK) [10] was developed to provide guidance capability for needle-based interventions including vertebroplasty, lung biopsy, and lung RFA. In that work, we performed an animal survival study for lung RFA and two navigation measures were evaluated in [10] including the execution time to reach target and distance from target. The mathematical model used for planning was similar to the current one, but we only provided the physician with a single "optimal" plan based on the problem formulation. We now build upon this prior work to develop a comprehensive planning, evaluation, and execution system. Instead of providing a single plan, we present the physician with a number of feasible plans from which they select one based on their preference with regard to the importance of the quantitative evaluation measures. In the clinical practice of our interventional radiologist, RFA probe placement is performed under CT-fluoroscopy in a freehand manner. The probe repositioning is likewise performed by the mental triangulation of the interventional radiologist. After the initial ablation, the tissue imaging characteristics around the tumor change in real time due to physiologic phenomena such as hyperemia, nitrogen gas release during ablation, etc. The tumor margins almost always become obscured. Therefore, it is almost impossible for the interventional radiologist to plan overlapping ablations by hand, which motivated the integrated system development described here.

III. Methods

A. System Overview

The overall system concept is shown in Fig. 1, with the key components including treatment optimization, treatment

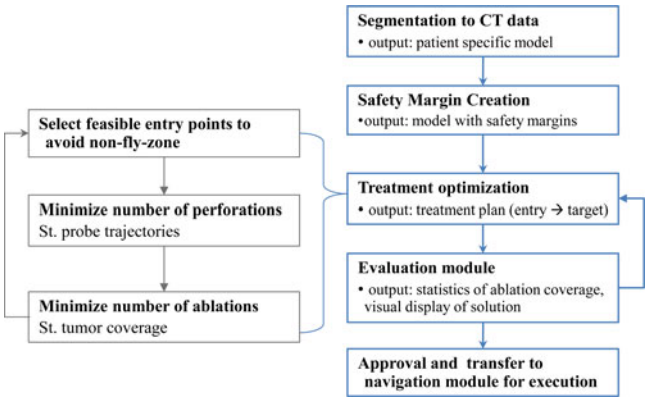

Fig. 2. Treatment planning flowchart.

evaluation, and surgical navigation. Specifically, the planning workstation implements patient-specific modeling through segmentation, margin addition, optimization, and plan evaluation as illustrated in Fig. 2.

Semiautomatic segmentation based on geodesic active contour method [17] is used to identify the key structures including: the tumor; structures that should not be traversed such as the ribs, liver vasculature, and adjacent critical anatomical structures, collectively referred to as a no-fly-zone; and surgeon preferred entry points.

Additional margins are created for tumor tissue, ablation margin, and critical tissue, which includes safety margins that should be avoided. This is realized by applying a binary image morphological operator, dilation, to the segmented tumor and critical structures.

Following the flowchart given in Fig. 2 and notations in Table I, we next describe the optimization-based planning and the evaluation modules.

B. Treatment Planning Including Path Planning and Overlapping Optimization

As illustrated in Fig. 2, a semiautomatic treatment planning module for optimized probe placement is developed to guide the RFA ablation probe. For a given irregular liver tumor, the solution of a mathematical optimization problem provides 1) optimized probe trajectories, 2) location of multiple overlapping ablations in order to cover the tumor, and 3) a tumor-free margin, while avoiding the no-fly zone. Hence, the treatment planning is a multiple-objective optimization problem guided by the following five clinical considerations.

1) Minimize the number of ablations. Fewer ablations mean shorter treatment times and less chance for complications.
2) Limit the number of probe insertions. This reduces the perforations to the liver capsule decreasing the chances of intraperitoneal haemorrhage.
3) Probe trajectory constraints. The model includes physical constraints imposed by ribs, vessels, and other organs which restrict possible trajectories.
4) Irregular shaped tumor coverage. The optimization uses segmented tumor data from patients and does not presuppose a particular tumor shape. This makes this planning method more general.
5) Minimize unnecessary damage to healthy tissue while fully covering the tumor and margin.

TABLE I
NOMENCLATURE

Symbol	Quantity	Notes
R	RFA probe radius	in millimeter, 15 mm in this article
T	Set of tumor points	denoted by a set of spatial voxels
TR	Set of trajectories, t	
M	Set of ablation margin points	denoted by a set of spatial voxels
$K(t,c)$	=1 if trajectory t can cover cell c	indicates the coverage provided by trajectory t
c	Cell to be ablated	denoted by a spatial voxel
y_a	Binary variable corresponding to an ablation centered at a	$y_a = 1$, if ablation centered at a; $y_a = 0$, otherwise
x_t	Binary decision variable corresponding to trajectory t	$x_t = 1$, if trajectory t is selected; $x_t = 0$, otherwise
A	Set of candidate points for ablation centers	

The optimization module uses integer programming techniques to model and solve the planning problem. Considering a voxelized tumor region, the possible choices for trajectories and ablations are represented by binary decision variables and the clinical constraints are modeled algebraically using linear inequalities [18]. This methodology has also been applied for radiotherapy treatment planning problems involving brachytherapy [19], [20].

Aiming at optimizing multiple measures of RFA planning performance simultaneously, we present a decomposition approach that solves this decision problem by repeatedly solving two integer programming models. Initially, a set of entry points is specified by the clinician and each entry point is tested for feasibility in avoiding direct puncture of critical structures to the tumor. Then, for each feasible entry point, we define the following two optimization models: the minimal trajectories integer program (MTIP) to find a minimal number of trajectories necessary to cover the tumor, and the minimal ablations integer program (MAIP) to find a minimal number of ablations along the selected trajectories necessary to cover the tumor. In each of these integer programs, we employ a weighted formulation to reduce healthy tissue damage, while keeping as main objective the minimization of the number of trajectories and ablations that are needed to guarantee coverage of the tumor and safety margin.

1) *MTIP is*

$$\begin{aligned} &\min \sum_{\{t \in TR\}} w_t\, x_t \\ &\text{subject to} \sum_{\{t:K(t,c)=1\}} x_t \geq 1 \;\forall c \in T \cup M \\ &x_t \in \{0,1\} \quad \forall t \in TR \end{aligned} \tag{1}$$

where x_t is the binary decision variable indicating if a candidate trajectory is used or not, *TR* is the set of candidate trajectories, T is the set of tumor points, and M the set of margin points. Since individual trajectories may cover a partial tumor volume; the weight w_t is used to indicate the penalty associated with each trajectory. By default, their values can all be set equal to 1 (or to any other constant). In this case, the objective function looks for a smallest set of directions that can cover the target region. Alternatively, a trajectory can be given additional weight if it covers a volume of healthy tissue. For example, we can choose $w_t = 1 + 0.01\ p_t$, where p_t is the proportion of healthy cells among the cells ablated if trajectory t were chosen. The portion of the weight associated with healthy tissue damage ($0.01\ p_t$) is orders of magnitude smaller than the unit weight assigned to using the direction t. This preserves the main goal of minimizing the total number of trajectories needed while penalizing the use of trajectories that ablate more healthy tissue. The constraints in the model assure that each tumor or margin point is covered by at least one suitable trajectory. The function $K(t, c) = 1$ if trajectory t can cover cell c, indicates the coverage provided by trajectory t. We model the region that a probe trajectory can ablate as a cylinder with axis along the trajectory and radius smaller than the radius of a single ablation.

2) *MAIP is formulated as*

$$\begin{aligned} &\min \sum_{\{a \in A\}} w_a\, y_a \\ &\text{subject to} \sum_{\{a:\|a-c\|<R\}} y_a \geq 1\ \forall c \in T \cup M \\ &y_a \in \{0,1\}\ \forall a \in A \end{aligned} \tag{2}$$

where A is the set of proposed ablation centers. The points in the set A are generated along the set of trajectories obtained from solving MTIP. As before, T is the set of tumor points, and M the set of margin points. The constraints in the model require that each tumor or margin point be covered at least once by an ablation. The weights w_a can be chosen to minimize the number of ablations as main goal and, simultaneously, reduce healthy tissue damage by giving more weight to an ablation if it covers a larger volume of healthy tissue. Similar to the weights in MTIP, we can choose $w_a = 1 + 0.01\ p_a$, where p_a is the proportion of healthy cells among the cells ablated if an ablation centered at point a is selected. By using the condition $\|a - c\| < R$, we are assuming that ablations are spherical. We did this because spheres are commonly used to model ablations in the literature and it also simplified the software implementation for our computational experiments. However, ablations that vary arbitrarily in shape at each possible placement point can just as well be represented in the MAIP model. Finally, we note that finding an optimal solution to an integer program can be computationally very challenging. To solve our integer programming models, we used Gurobi version 4.0.2, an optimization package with the branch and bound algorithm [18]. Since the original decision problem was decomposed into two subproblems, the solutions that we obtain are not guaranteed to be globally optimal. Our computational experiments, discussed later, show that the solutions obtained are of good quality and useful in a clinical setting.

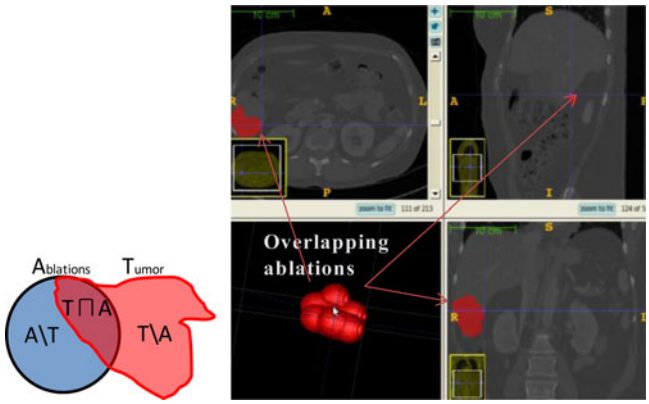

Fig. 3. (Left) Venn diagram illustrating the evaluation measures by regional overlapping of ablations (A) and tumor (T). (Right) Model of multiple overlapping ablations generated from treatment plan. (Refer to the web version of this paper for the color figure.)

C. Evaluation Measures

After the candidate plans are generated by the optimizer, statistical evaluation on the quality of the plans is further developed. Assuming each ablation covers a spherical region, the model with multiple ablations can be generated from the treatment plan as in Fig. 3 (Right). Given the multiple spherical planned ablations and tumor model in Fig. 3 (Left), the evaluation measures are defined by

1) Ablation Coverage (AC): AC = A ∩ T/T;
2) Unablated Percentage (UP): UP = (T\A)/T;
3) Over-Ablation (OA) Volume:
   OA = (Ablation Volume)* (A\T)/A, in mm^3;
4) NA: Number of Ablations;
5) NT: Number of Trajectories.

IV. Experimental Evaluation

A. Phantom Study

An abdominal CT of a torso phantom [see Fig. 4(a)] was obtained in the Radiology Department. Then, a semiautomatic segmentation [see Fig. 4(b)] was done to obtain an anatomical model, particularly, the structures of tumor, ribs, entry points, and no-fly-zone. Given identified structures, the planning algorithm generates needle trajectories and ablation locations represented by pink spheres (see electronic version) to show the coverage on the whole tumor. Finally, the intervention is carried out using a navigation program based on the IGSTK, with electromagnetic tracking of the probes.

The planning system allows the user to fix the values of key decision variables in the model prior to executing the optimization algorithm, as shown in Fig. 5. Prior to the execution of the optimization algorithm, it allows the user to manually input criteria that must be satisfied by the solutions, such as probe information, patient sample data spacing, maximal number of ablations, maximal number of trajectories, maximal number of punctures, and tumor margin. This feature is also used to

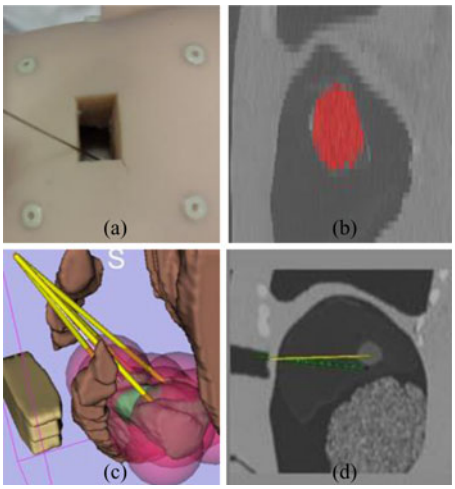

Fig. 4. Ablation planning and navigation. (a) Phantom with markers. (b) Chest CT scan and tumor segmentation in red. (c) Treatment planning (yellow line: RFA probe; green: tumor; pink sphere: ablations; brown: non-fly-zone; green: tumor to be ablated). (d) Navigation screenshot in IGSTK. (Refer to the web version of this paper for the color figure.)

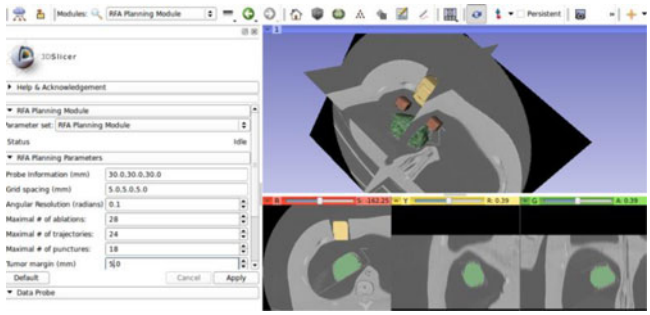

Fig. 5. Open-source RFA planning module implemented in 3-D slicer. (Refer to the web version of this paper for the color figure.)

TABLE II
STATISTICAL MEASURES FOR THE CANDIDATE PLANS FOR TUMOR SIZE OF 35-mm DIAMETER

Plan ID	AC	OA (mm^3)	NA	NT
1	0. 991	46580	6	3
2	0.984	39838	6	3
3	0.988	47131	7	3
4	0.987	44899	7	3

iteratively update the treatment plan after each actual insertion and ablation is realized.

For simulation purposes, two types of simulated tumors were used, including a spherical one and a cylindrical one, which do not represent real pathological examples but demonstrate algorithmic feasibility. The ablation probe used in this experiment has an ablation sphere of 30 mm in diameter.

For a simulated spherical tumor with 35-mm diameter, the planning system generated four candidate treatment plans with an average ablation coverage rate of 99% and over-ablation rate of 40% as shown in Table II. For a simulated cylindrical shape tumor with 65-mm long and 45-mm diameter, ten treatment plans were generated with an average ablation coverage rate of 98% and over-ablation rate of 44%. The phantom experiments demonstrate that the planning approach is able to generate feasible treatment plans effectively. Multiple ablations can be constrained along the same trajectory to reduce the number of punctures. Note that while these experiments demonstrate the feasibility of the proposed approach for large tumors, such a large number of ablations would not be practical in current clinical practice.

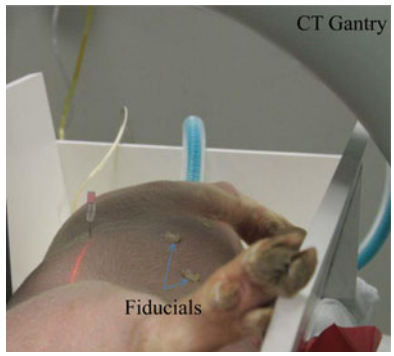

Fig. 6. Preoperative experiment setup including animal placed in V-trough under general anaesthesia, fiducial marker placement, and CT scan.

B. Animal Study

1) Preoperative Experiment Setup: A swine study was completed to validate the system feasibility in clinical environment. A 40-kg swine was used under an approved animal protocol of the Guide for the Care and Use of Laboratory Animals. The *in vivo* tumor-mimicing model was prepared using a mixture of agarose, cellulose, glycerol, and methylene blue as described in [21]. Under general anesthesia, an artificial tumor was created by injecting the prepared agar in the liver percutaneously under CT guidance. Six surface fiducial markers were placed on the abdomen for later use in paired-point registration. A volumetric CT scan was then performed using a Siemens Somatom Emotion 16 CT Scanner system to obtain the preoperative images for planning and navigation. The preoperative experiment setup is shown in Fig. 6.

Similar to the workflow of the phantom study described earlier, the CT data with dimension of $512 \times 512 \times 301$ and spacing of $0.58 \times 0.58 \times 1$ mm were then transferred to the planning workstation, where the segmentation and ablation planning were performed. The semiautomatic segmentation took 6 min to generate the models of tumor, rib, and entry points (in Fig. 7) as validated by the radiologists. An ablation margin of 5 mm [22] was created around the tumor. This results in an ablation region whose long axis is approximately 35 mm, which requires multiple ablations for complete coverage.

2) Treatment Planning Experiment Results: Interventional planning was then applied to the preoperative model of key anatomical structures, such as tumor, safety margin, ribs, and entry regions. Together with visualization and ablation coverage evaluation, the whole planning procedure took 3 min and generated 15 candidate plans as shown in Table III.

The ablation coverage on the tumor is 100%, average coverage on the tumor with margin is 99.05%, average over-ablation

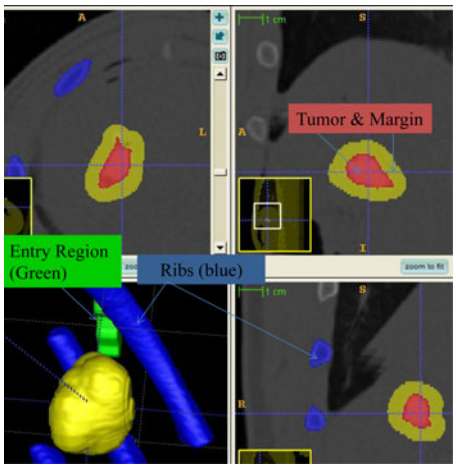

Fig. 7. Preoperative CT scan overlaid by tumor region, ribs, preferred ablation probe entry region and safety margin. The region with red denotes the tumor within liver. Green represents the entry region and blue for no-fly-zone. (Refer to the web version of this paper for the color figure.)

TABLE III
STATISTICAL MEASURES FOR THE CANDIDATE PLANS FOR SIMULATED TUMOR SIZE OF 25-mm DIAMETER

Plan ID	AC	OA (mm^3)	NA	NT
1	0.980	8067	3	2
2	0.989	6710	2	2
3	0.989	6710	2	2
4	0.981	7497	2	2
5	1	8337	2	2
6	0.999	8452	2	2
7	0. 999	8416	2	2
8	0. 999	8598	2	2
9	0. 986	8403	2	2
10	0. 992	6910	2	2
11	0.992	6910	2	2
12	0. 996	8653	2	2
13	0. 995	8368	2	2
14	0. 991	6630	2	2
15	0. 980	8067	2	2

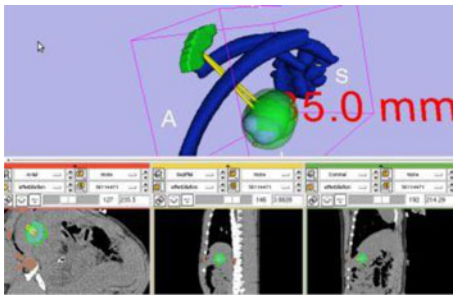

Fig. 8. Treatment plan visualization module for surgeons to evaluate the plan before execution. The long axis is approximately 35 mm calculated by Slicer's measurement module (www.slicer.org). The planned ablation spheres were overlaid onto the preoperative CT images as shown in the three lower slice views, which make it easy to examine slice-by-slice performance. (Refer to the web version of this paper for the color figure.)

rate is 45.99%, and two ablations were required. This validated the proposed planning algorithm and was confirmed by the radiologist. Fig. 8 visualizes the planned ablation coverage in 3-D slicer [23] using our implemented multiple plan visualization module, which can load in multiple plans for visual comparison. The visibility of individual candidate plans can be toggled ON or OFF in 3-D view and slice view for comparison. Within the same spatial coordinate system, the raw CT DICOM series, the multiple treatment plans, the segmented structures and measurements can be overlaid in the same workspace, which is preferred by the radiologists.

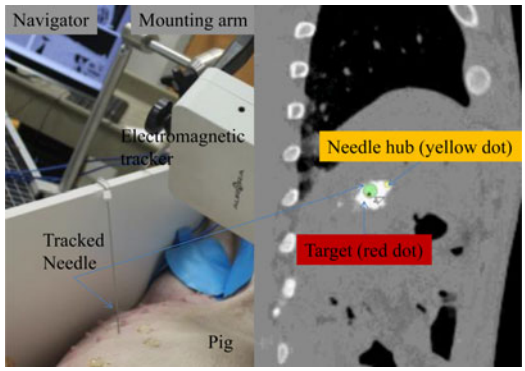

Fig. 9. (Left) Navigation setup and (right) navigator projected view. (Refer to the web version of this paper for the color figure.)

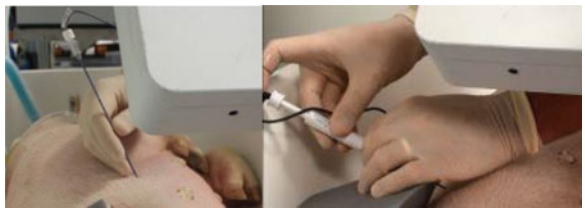

Fig. 10. Procedure of ablation probe deployment: tracked needle insertion on the left picture, and probe deployment on the right picture.

3) Ablation Under Image Guidance: The ablation plan with highest tumor coverage rate was selected for execution under image guidance. The navigation experiment setup is shown in Fig. 9, which shows the electromagnetic tracking system used for image guidance. The tracked needle was registered to preoperative image space via paired-point registration with a fiducial registration error of 3.8 mm. The navigation module was implemented based on the IGSTK and the needle pose (position and orientation) relative to image space was presented in the navigator. A projected view is shown in Fig. 9, which denotes the relative orientation of needle hub, needle tip, and target point in image space. The 16-gauge tracked trocar and needle was then navigated to the target lesion. The ablation probe (Boston Scientific, Natick, MA, USA) was inserted along the trocar to the target, and then, the RFA was applied by turning on the radiofrequency generator, as shown in Fig. 10.

After the second ablation was completed, the probe was left in place and the swine was moved back to the CT scanner for a postoperative evaluation. The scan has an image dimension of $512 \times 512 \times 155$ slices and spatial spacing of $0.67 \times 0.67 \times 1$ mm. Due to the pig position and acquisition parameters had been changed, the postoperative scan could not be directly overlaid to preoperative scan or treatment plans for computation. Alternatively, we segmented the tumor and applied a safety margin again. Meanwhile, we manually identified the ablation sphere with a radius of 15 mm as shown in Fig. 11 (left), which

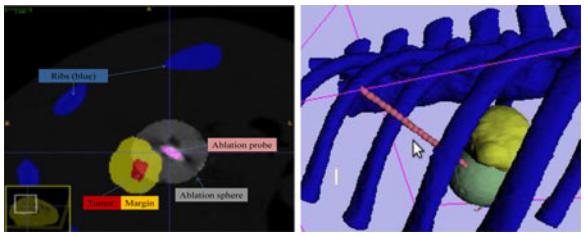

Fig. 11. (Left) Postoperative CT scan to check the spatial relationship between the ablation probe with the region of tumor and safety margin. The virtual ablation sphere is generated via image processing cantered at the probe tip and then overlaid onto the postoperative CT scan. The distance of delivered probe to tumor surface is approximately 5 mm. (Right) Postoperative evaluation on the second accomplished RFA. Yellow color represents the tumor surrounded by safety margin and the sphere denotes the virtual ablation. (Refer to the web version of this paper for the color figure.)

shows overlapping region between the tumor margin and actual ablations. The target ablation coverage by the second ablation is 34% by calculation of the ratio of overlapping ablation over the total tumor and margin volume. Fig. 11 (right) demonstrates that the second needle insertion avoids the ribs and reaches the target tumor.

C. Discussion

The planning module yielded 100% coverage over the large tumor using multiple ablations and can generate multiple feasible plans (e.g., Table III for animal study) with evaluation parameters for physicians to choose. Both numerical evaluation and visual evaluation (e.g., Fig. 8) can be performed to determine the execution plan from those candidates. The number of trajectories and ablations are reduced to a minimum at the same time. In our previous approach for planning ablations for lung tumors [10], we only generated an "optimal" solution, which removed the specific perspective of the interventionalist. We now provide the physician with multiple feasible plans that satisfy to some degree the optimization requirements. This is a cooperative approach to planning in which the computational burden is automated, and the clinician selects from a small set of plans which satisfy the clinical criteria such as maximum number of trajectories, maximum number of ablations, overlap of ablation spheres, etc.

This approach yields comprehensive and clinically feasible planning results. Given the requirement of 100% coverage on the tumor, the over-ablation rate is found relevant to the size and shape of the tumor, the size of ablation probe and the maximum number of ablations. As illustrated in Fig. 12, even one ablation can result in a high over-ablation rate if the tumor is far smaller than the spherical coverage. Similarly in the animal study, the long axis of the ellipsoidal tumor is slightly bigger than probe diameter and the short axis is much shorter than the probe diameter, which can result in the two ablations covering more healthy tissue. The over-ablation rate can be decreased using a smaller probe size and a larger number of ablations. Hence, physicians can consider the tradeoff between over-ablation and the allowable number of ablations.

The navigation module based on the electromagnetic tracking system is susceptible to interference from the CT scanner. In earlier phantom studies on the CT table directly, the fiducial

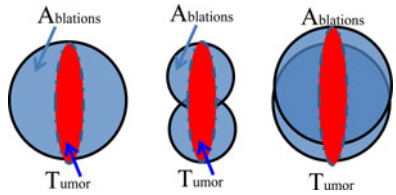

Fig. 12. Illustration of the factors effecting over-ablation including tumor shape and size, choices of ablation probe sizes, and maximum number of ablations. Left figure shows the bigger probe used only one ablation to cover the tumor, resulting in over-ablation of more than 60%. Middle figure achieves less over-ablation rate but uses more ablations. Right figures demonstrate the similar case as animal study where the balance of probe size and number of ablations needs to be determined.

registration error was up to 10 mm, which is too large for accurate targeting. Once we moved the phantom to a metal-free environment, the fiducial registration error could be decreased to 1 mm and yield accurate targeting performance. For this reason, in our animal study the swine was moved to a table in the CT room away from the CT gantry, where we were able to obtain a registration error from 3.6 to 3.9 mm for several trials. This makes the postoperative CT evaluation difficult for each ablation, as the animal cannot be moved back to CT and moved out for performing the subsequent planned ablations without potentially changing its position relative to the V-trough. The final targeting error is difficult to evaluate as the planned trajectory cannot be mapped to the postoperative image coordinate system. Instead, we measure the distance from the probe to the tumor margin region surface in 3-D slicer and found the distance from the probe to the closest tumor surface was approximately 5 mm. For the future study, a preoperative image to postoperative image registration method can be developed to overcome this limit in ablation evaluation.

According to the planning results and evaluation results on the second ablation, we show the feasibility of semiautomatic planning and navigation procedures overseen by the radiologist. The presented ablation planning and navigation approach provides a comprehensive solution for treating large tumors using RFA, while keeping the physician in the loop. The planning system uses a patient specific model and an optimization approach to produce potential plans that satisfy multiple clinical criteria to certain degrees. The clinicians then select the plan which they judge to be most appropriate. The navigation system provides the precise guidance required to carry out the plan, which currently is all but impossible to do using the standard free hand technique.

V. Conclusion

A new treatment planning and navigation system was developed for liver tumor ablations, particularly for multiple overlapping RFAs. The treatment planning is composed of needle-like probe trajectory planning and overlapping ablation planning. Multiple-objective optimization for probe insertions incorporates both clinical and technical constraints. Additional validation is required prior to introducing our system into a clinical trial. Systematic evaluations were presented to check the candidate plans by both statistical measures and visualization. The presented semiautomatic planning and guidance method can be

applied to tumor ablation in other organs using the proposed techniques. In its current form, the system in combination with a phantom can also be used as a training aid for interventional radiologists.

ACKNOWLEDGMENT

The authors would like to thank the assistance of L. Chauvin, A. Yamada, and S. Piper from Brigham Women's Hospital and Harvard Medical School in using 3-D slicer; the useful discussions with P. Cheng and O. Guler in using IGSTK; and animal care from J. Gnadt and R. Tucker in the Georgetown University.

REFERENCES

[1] R. Siegel, D. Naishadham, and A. Jemal, "Cancer statistics," *CA: A Cancer J. Clinicians*, vol. 62, no. 1, pp. 10–29, 2012.
[2] M. Howenstein and K. Sato, "Complications of radiofrequency ablation of hepatic, pulmonary, and renal neoplasms," *Semin. Intervent. Radiol.*, vol. 27, no. 3, pp. 285–295, 2010.
[3] E. Abdalla, J. Vauthey, L. Ellis, V. Ellis, R. Pollock, K. Broglio, K. Hess, and S. Curley, "Recurrence and outcomes following hepatic resection, radiofrequency ablation, and combined resection/ablation for colorectal liver metastases," *Ann. Surg.*, vol. 239, no. 6, pp. 818–827, 2004.
[4] T. G. Simon and D. E. Dupuy, "Radiofrequency ablation, microwave ablation, and cryoablation for lung tumors," in *Interventional Oncology*, P. Mueller and A. Adam, Eds. New York, NY, USA: Springer, 2012, pp. 149–159.
[5] J. P. McWilliams, S. Yamamoto, S. S. Raman, C. T. Loh, E. W. Lee, D. M. Liu, and S. T. Kee, "Percutaneous ablation of hepatocellular carcinoma: Current status," *J. Vascular Int. Radiol.*, vol. 21, no. 8 Suppl, pp. S204–S213, 2010.
[6] S. Goldberg, C. Grassi, J. Cardella, J. Charboneau, G. Dodd, II, D. Dupuy, D. Gervais, A. Gillams, R. Kane, F. Lee, Jr. *et al.*, "Image-guided tumor ablation: Standardization of terminology and reporting criteria1," *Radiology*, vol. 235, no. 3, pp. 728–739, 2005.
[7] T. Livraghi, S. Goldberg, S. Lazzaroni, F. Meloni, T. Ierace, L. Solbiati, and G. Gazelle, "Hepatocellular carcinoma: Radio-frequency ablation of medium and large lesions1," *Radiology*, vol. 214, no. 3, pp. 761–768, 2000.
[8] N. Nesher, M. Ben Haim, D. Pevni, A. Kessler, and Y. Paz, "Ultrasound-guided, video-assisted transdiaphragmatic radiofrequency ablation for primary liver malignancy or metastatic nodules," *Innovations: Technol. Techn. Cardiothoracic Vascular Surg.*, vol. 6, no. 5, pp. 337–340, 2011.
[9] J. Stoll, H. Ren, and P. E. Dupont, "Passive markers for tracking surgical instruments in real-time 3D ultrasound imaging," *IEEE Trans. Med. Imag.*, vol. 31, no. 3, pp. 563–575, Mar. 2012.
[10] Z. Yaniv, P. Cheng, E. Wilson, T. Popa, D. Lindisch, E. Campos-Nanez, H. Abeledo, V. Watson, K. Cleary, and F. Banovac, "Needle-based interventions with the image-guided surgery toolkit (IGSTK): From phantoms to clinical trials," *IEEE Trans. Biomed. Eng.*, vol. 57, no. 4, pp. 922–933, Apr. 2010.
[11] C. Baegert, C. Villard, P. Schreck, L. Soler, and A. Gangi, "Trajectory optimization for the planning of percutaneous radiofrequency ablation of hepatic tumors," *Comput. Aided Surg.*, vol. 12, no. 2, pp. 82–90, 2007.
[12] M. Chen, W. Yang, K. Yan, M. Zou, L. Solbiati, J. Liu, and Y. Dai, "Large liver tumors: Protocol for radiofrequency ablation and its clinical application in 110 patients mathematic model, overlapping mode, and electrode placement process," *Radiology*, vol. 232, no. 1, pp. 260–271, 2004.
[13] G. Dodd, M. Frank, M. Aribandi, S. Chopra, and K. Chintapalli, "Radiofrequency thermal ablation," *Amer. J. Roentgenol.*, vol. 177, no. 4, pp. 777–782, 2001.
[14] L. Yang, R. Wen, J. Qin, C. Chui, K. Lim, and S. Chang, "A robotic system for overlapping radiofrequency ablation in large tumor treatment," *IEEE/ASME Trans. Mechatron.*, vol. 15, no. 6, pp. 887–897, Dec. 2010.
[15] T. Butz, S. Warfield, K. Tuncali, S. Silverman, E. van Sonnenberg, F. Jolesz, and R. Kikinis, "Pre- and intra-operative planning and simulation of percutaneous tumor ablation," vol. 3, pp. 317–326, Oct. 2000.
[16] H. Zhang, F. Banovac, S. Munuo, E. Campos-Nanez, H. Abeledo, and K. Cleary, "Treatment planning and image guidance for radiofrequency ablation of liver tumors," in *Proc. SPIE*, 2007, vol. 6509, pp. 650922-1–650922-10.
[17] P. Yushkevich, J. Piven, H. Hazlett, R. Smith, S. Ho, J. Gee, and G. Gerig, "User-guided 3D active contour segmentation of anatomical structures: Significantly improved efficiency and reliability," *Neuroimage*, vol. 31, no. 3, pp. 1116–1128, 2006.
[18] L. Wolsey, *Integer programming*. New York, NY, USA: Wiley, 1998.
[19] E. Lee, R. Gallagher, D. Silvern, C. Wuu, and M. Zaider, "Treatment planning for brachytherapy: An integer programming model, two computational approaches and experiments with permanent prostate implant planning," *Phys. Med. Biol.*, vol. 44, pp. 145–165, 1999.
[20] W. D'Souza, R. Meyer, B. Thomadsen, and M. Ferris, "An iterative sequential mixed-integer approach to automated prostate brachytherapy treatment plan optimization," *Phys. Med. Biology*, vol. 46, pp. 297–322, 2001.
[21] D. Scott, W. Young, L. Watumull, G. Lindberg, J. Fleming, R. Rege, R. Brawn, and D. Jones, "Development of an in vivo tumor-mimic model for learning radiofrequency ablation," *J. Gastrointestinal Surg.*, vol. 4, no. 6, pp. 620–625, 2000.
[22] K. Yamakado, A. Nakatsuka, S. Ohmori, K. Shiraki, T. Nakano, J. Ikoma, Y. Adachi, and K. Takeda, "Radiofrequency ablation combined with chemoembolization in hepatocellular carcinoma: Treatment response based on tumor size and morphology," *J. Vascular Int. Radiol.*, vol. 13, no. 12, pp. 1225–1232, 2002.
[23] S. Pieper, M. Halle, and R. Kikinis, "3D slicer," in *Proc. IEEE Int. Symp. Biomed. Imag.: Nano to Macro*, 2004, pp. 632–635.

Hongliang Ren (M'06) received the Ph.D. degree in electronic engineering (Biomedical Engineering Lab) from the Chinese University of Hong Kong, Hong Kong, in 2008.

He is currently an Assistant Professor and leading a research group on medical mechatronics in the Biomedical Engineering Department, National University of Singapore (NUS), Singapore. He worked as a Postdoctoral Researcher in the Laboratory for Computational Sensing and Robotics (LCSR) and the Engineering Center for Computer-Integrated Surgical Systems and Technology (ERC-CISST), Department of Biomedical Engineering and Department of Computer Science, The Johns Hopkins University, Baltimore, MD, USA, from 2008 to 2010. In 2010, he joined the Pediatric Cardiac Biorobotics Lab, Department of Cardiovascular Surgery, Children's Hospital Boston & Harvard Medical School, USA, for investigating the beating heart robotic surgery system. Prior to joining NUS, he also worked in 2012 on a collaborative computer integrated surgery project, at the Surgical Innovation Institute of Children's National Medical Center, Washington, DC, USA.

Enrique Campos-Nanez received the B.Sc. degree in mathematics from the Universidad Nacional Autónoma de México (UNAM), Mexico, the M.Sc. degree in operations research from Stanford University, Stanford, CA, USA, and the Ph. D. degree in systems and information engineering from the University of Virginia, Charlottesville, VA, USA.

He is currently a Senior Software Engineer at The Epsilon Group, an Alere Inc. company, Charlottesville, VA, USA, where he is a Development Lead on the company's modeling and simulation software for pharmacokinetics. His research interests include healthcare analytics, mathematical modeling in medicine, and systems and software engineering.

Ziv Yaniv (M'04) received the Ph.D. degree in computer science from The Hebrew University of Jerusalem, Jerusalem, Israel, in 2004.

He is a Principal Investigator at the Sheikh Zayed Institute for Pediatric Surgical Innovation, Children's National Hospital, Washington, DC, USA. His main research interests are image-guided interventions, medical image analysis, computer vision, and software engineering. He actively supports the development of open source software, and leads the development of the free open source Image-Guided Surgery Toolkit (IGSTK).

Dr. Yaniv is a member of the IEEE Engineering in Medicine and Biology and IEEE Computer societies.

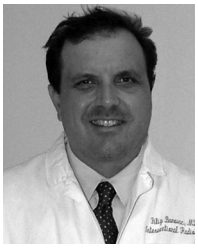

Filip Banovac received the B.S.E. degree in biomedical engineering from Duke University, Durham, NC, USA, followed by the Medical degree from the Medical College of Virginia, Richmond, VA, USA and the Clinical Residency Training in radiology and interventional radiology from Georgetown University, Washington, DC, USA and Stanford University, Stanford, CA, USA, respectively, in 2003 and 2004.

He is currently the Chief of Vascular and Interventional Radiology at Georgetown University Hospital, Washington. His research interests include the field of image guided navigation and targeting for tissue ablation of liver and lung tumors.

Hernan Abeledo received the Ph.D. degree in operations research from Rutgers University, New Brunswick, NJ, USA, in 2003.

He is an Associate Professor at the Department of Engineering Management and Systems Engineering, George Washington University, Washington, DC, USA. His main research interests are mathematical optimization and operations research applications.

Nobuhiko Hata received the B.E. degree in precision machinery engineering in 1993, the M.E. degree in 1995, and the Doctor of Engineering degrees in 1998 from the University of Tokyo, Tokyo, Japan.

He is currently an Associate Professor of Radiology, Harvard Medical School and Brigham and Women's Hospital, Boston, MA, USA. In the Image Guided Therapy Program and Surgical Navigation and Robotics Laboratory at Brigham and Women's Hospital, he leads research team on medical image processing and robotics in image-guided surgery. His major achievements include neurosurgical navigation combined with ultrasound imaging, surgical robot for magnetic resonance imager, and motion-adaptable surgical robot for image-guided therapy.

Kevin Cleary (M'86) received the B.S. and M.S. degrees in mechanical engineering and materials science from the Duke University, Durham, NC, USA, followed by the Ph.D. degree from the University of Texas, Austin, TX, USA.

He was an NSF-sponsored Postdoctoral Researcher at the Mechanical Engineering Laboratory, Tsukuba, Japan. He is currently the Technical Director of the Bioengineering Initiative in the Sheikh Zayed Institute for Pediatric Surgical Innovation, Children's National Medical Center, Washington, DC, USA. He leads a research team developing technology to make pediatric surgery more precise and less invasive, including robotics, navigation, and image fusion.